He *et al.*
Chinese Journal of Mechanical Engineering (2022) 35:31
https://doi.org/10.1186/s10033-022-00699-z

Chinese Journal of Mechanical Engineering

ORIGINAL ARTICLE Open Access

A Φ 6-m Tunnel Boring Machine Steel Arch Splicing Manipulator

Yuanfu He[1,2], Yimin Xia[1,2*], Zhen Xu[3], Jie Yao[4,5], Bo Ning[1,2] and Xuemeng Xiao[1,2]

Abstract

Robotic splicing of steel arches is a challenging task that is necessary to realize the grasping and docking of steel arches in a limited space. Steel arches often have a mass of more than 200 kg and length of more than 4 m. Owing to the large volume and mass of steel arches and the high requirements for accurately positioning the splicing, it is difficult for a general manipulator to meet the stiffness requirements. To enhance the structural stiffness of the steel arch splicing manipulator, a single-degree-of-freedom (DOF) closed-loop mechanism was added to the grasping structure of the manipulator. Based on the basic principle of structural synthesis, a solution model of the single-DOF closed-loop mechanism was developed, and alternative kinematic pairs of the mechanism with different input constraints and output requirements were derived. Based on this model, a design method for a single-DOF closed-loop grasping mechanism and a posture adjustment mechanism for a steel arch was devised. Combined with the same dimensional subspace equivalence principle of the graphical-type synthesis method, 12 types of steel arch splicing manipulator were constructed. By analyzing the motion/force transmission and structural complexity of the steel arch splicing manipulators, the best scheme was selected. A prototype of the steel arch splicing manipulator was manufactured. Adams software was used to obtain clearly the output trajectory of the end of the manipulator. The relative spatial positions of the upper and lower jaws under different working stages were analyzed, demonstrating that the manipulator satisfied the grasping requirements. Through a steel arch splicing experiment, the grasping effect, docking accuracy, and splicing efficiency of the manipulator met the design requirements. The steel arch splicing manipulator can replace the manual completion of the steel arch splicing operation, significantly improving the operation efficiency.

Keywords: Steel arch splicing manipulator, Single-DOF closed-loop mechanism, Screw theory, Graphical-type synthesis method, Mechanism design

1 Introduction

Generally known as large-scale equipment, the hard rock tunnel boring machine (TBM) is used to excavate tunnels inside hard rock [1–4]. With the functions of excavating, slagging, and supporting, the TBM has been widely adopted in the field of hard rock excavation [5–7]. The TBM unavoidably destroys the initial in situ stress state of the surrounding rock in the original stratum, resulting in the redistribution of stress in the surrounding rock, which leads to the deformation, destruction, or even collapse of the surrounding rock [8, 9]. When the quality of the surrounding rock is unsatisfactory and the fragmentation of the rock mass is severe, the self-stabilization period of the surrounding rock is quite short or fails to appear. Therefore, it is necessary to provide timely and effective steel arch support to control the deformation of and prevent damage to the surrounding rock [10, 11]. At present, splicing of TBM steel arches is performed manually, as shown in Figure 1. Inside a narrow operation area for construction personnel, the working environment is extremely harsh, with strong vibration, numerous dust particles, low brightness, and high humidity, where laborers are

*Correspondence: xiaymj@csu.edu.cn
[1] College of Mechanical and Electrical Engineering, Central South University, Changsha 410083, China
Full list of author information is available at the end of the article

a Construction environment **b** Docking process

Figure 1 Manual splicing of steel arch

often required to stand in stagnant water. Each steel arch weighs up to 200 kg and requires manual movement, adjustment, and docking. The extreme difficulty of the process can lower the splicing efficiency of the steel arch; furthermore, it can lead to untimely support or unstable quality and finally cause collapse accidents.

Currently, steel arch installation is mainly performed by manual coordination with a ring beam erector. The steel arches are delivered to the ring beam erector by a transport truck and TBM crane, and workers transport the steel arch to the assembly ring of the ring beam erector and fix it. The assembly ring then rotates at a certain angle to place the second steel arch. Workers adjust the attitudes of the adjacent steel arches on the assembly ring so that the two steel arches are close to each other. The bolt holes are aligned, and then they are bolted together. Because the steel arch is very heavy, it is difficult to grasp and drag, so many people are often required to carry and adjust the steel arch and even use jacks to assist in joining the steel arch, which seriously affects the construction efficiency. To relieve the workload and improve constructional quality, efficiency, and safety, the concept of automatic installation of TBM steel arches is proposed. A steel arch splicing manipulator was designed to realize the automatic splicing of steel arches and improve the intelligence and assembly efficiency of TBM construction.

Because this is the first reported investigation of the TBM steel arch splicing manipulator, related achievements have not been reported publicly, although a series of studies can be found associated with the design of the grasping manipulator [12]. Huang et al. [13] proposed a general design method for spatial three-degree-of-freedom (3-DOF) isotropic manipulators and developed six-degree-of-freedom (6-DOF) or redundant manipulators by applying 3-DOF robots as modules. Considering the operation and grasping requirements of the mechanism, Ozgür et al. [14] and Lambert et al. [15] analyzed the degree of freedom (DOF) and structure of planar and space manipulators and designed a manipulator with satisfactory grasping performance. Gao et al. [16] and Liang et al. [17] considered the shape diversity of a grasped object and designed a manipulator to realize a self-adaptive enveloping grasp. Kaluarachchi et al. [18] presented a design method for a lightweight tendon-driven redundant manipulator. With the joint torque reduced by applying a single motor, the number of actuators can be reduced, and power consumption can be minimized. Babin et al. [19] proposed a design method for manipulators that can grasp small objects within confined spaces by applying a planetary gear train to replace traditional revolute joints. However, despite the large mass, the steel arch has a slender I-beam structure. Therefore, owing to the inability to guarantee the grasping stability and docking accuracy of the steel arch, these design schemes are unsuitable for splicing steel arches.

The action of grasping a steel arch requires two jaws to cooperate with each other. To improve the dynamic performance, increase the structural stiffness, and reduce the input control, a single-DOF closed-loop planar mechanism was introduced into the grasping structure of the manipulator. At present, research on single-DOF closed-loop mechanismsmechanism is mainly focused on the leg and gripper mechanisms [20]. Studies of closed-loop planar mechanisms, such as the Chebyshev mechanism [21], Klann mechanism [22], LARM BiPED mechanism [23], and DQV [24], have shown that the closed-loop series structure possesses integral rigidity and is more suitable for missions under a high load. It also performs better at high stride frequency [25, 26]. Liu et al. [27] designed a single-DOF robot leg mechanism intended for tailed-quadruped locomotion. The design employs a four-bar planar mechanism that couples the hip and knee flexion/extension joints mechanically, thereby reducing the DOF of the leg without violating the foot trajectory. The actuator was concentrated at a proximal location, thereby increasing the rigidity-to-weight ratio. Hassan et al. [28, 29] introduced a crank slider mechanism into the gripper, realizing the purpose of a single driver controlling the tensioning of four fingers simultaneously. Anwar et al. [30] proposed a soft closed-chain modular gripper and designed a single-DOF closed-loop plane structure on each finger so that it can passively adapt to a curved surface, with the benefits of flexibility, low weight, and controllability. However, most of the above work is dedicated to the reconfiguration analysis of individual mechanisms and designs that combine existing mechanisms [31]. The fundamentals for the structural synthesis of a single-DOF closed-loop mechanism have not been systematically explored. No mathematical model that can serve as a basic modular foundation block for exploring similar closed-chain manipulators and grippers has been derived.

Among the innovative design theories and methods of articulated rigid-body systems, screw theory [32–35] and a graphical-type synthesis method [36, 37] have unique advantages in the design of complex manipulators because of their simple and intuitive characteristics; however, they are currently only used in the design of parallel manipulators. The grasping action of the steel arch splicing manipulator requires mutual cooperation between the upper and lower jaws as well as the functions of adjusting and docking the steel arch. Regarding this complex manipulator with multiple interrelated output tips, screw theory and the graphical-type synthesis method can realize the analysis and synthesis of the manipulator based on the basic principle. Currently, little research has been conducted in this field.

In this study, a solution model of a single-DOF closed-loop planar mechanism is presented. It is used to analyze the law of the number of kinematic pairs, arrangement, and axis layout of the mechanism. Based on this model, a design scheme for a single-DOF closed-loop grasping mechanism and a posture adjustment mechanism for a steel arch were developed. A steel arch splicing manipulator that can realize automatic installation of a steel arch was developed, and the reliability of the manipulator was verified experimentally.

2 Solution Model of Single-DOF Closed-Loop Mechanism

2.1 Analysis of Single-DOF Closed-Loop Mechanism

The mobility of a mechanism is generally calculated in terms of the Chebychev–Grübler–Kutzbach criterion [38], expressed as

$$F = d(n - g - 1) + \sum_{i=1}^{g} f_i, \tag{1}$$

where F is the mobility of the mechanism, d is the DOF of the space in which the mechanism works, n is the number of bodies connected by g joints, and f_i is the connectivity or DOF of the ith joint.

The single-DOF closed-loop mechanism is composed of rotating and moving pairs with one-DOF $(f_i{=}1)$. The numbers of bars n and kinematic pairs g must be equal, that is,

$$g{=}d + 1. \tag{2}$$

Screw theory is used to analyze the single-DOF closed-loop mechanism. Screw $\$_{Ri}$ of the ith revolute pair and screw $\$_{Pj}$ of the jth prismatic pair on the mechanism are expressed as

$$\$_{Ri} = \left(\boldsymbol{s}_{Ri};\ \boldsymbol{s}_{0_{Ri}} \right), \tag{3}$$

$$\$_{Pj}{=}\left(\mathbf{0};\ \boldsymbol{s}_{Pj} \right). \tag{4}$$

The sum of the spatial DOF d and the overconstrained number λ of the single-DOF closed-loop mechanism is six. If the virtual work done by the overconstrained screws in the single closed-loop mechanism on the motion-screw system is zero, then such an overconstraint does not affect the motion of the mechanism, thus ensuring the correctness of the mechanism.

If the motion-screw system of the mechanism is set as $\boldsymbol{S}{=}\left\{\$_1; \$_2; \cdots; \$_g\right\}$, and the constraint-screw system is set as $\boldsymbol{S}_r{=}\left\{\$_{r1}; \$_{r2}; \cdots; \$_{r\lambda}\right\}$, then, for $\forall k \in \{1, 2, \cdots, \lambda\}$ and $\forall j \in \left\{1, 2, \cdots, g\right\}$, the virtual work done by the kth constraint screw of the single closed-loop mechanism on the jth motion screw is derived as

$$\delta W{=}\ \$_j \circ \$_{rk} = 0. \tag{5}$$

The overconstraints are divided into independent force constraints and independent couple constraints, and the kinematic pairs are divided into revolute and prismatic pairs. According to Eq. (5), the virtual work should satisfy the following two conditions.

$$\begin{cases} \boldsymbol{s} \circ \boldsymbol{s}_r = \cos\alpha = 0, \\ \boldsymbol{s} \circ \boldsymbol{s}_{0r} + \boldsymbol{s}_r \circ \boldsymbol{s}_0 = -a\sin\alpha = 0, \end{cases} \tag{6}$$

where α and a are the spatial angle and distance between the motion screw and the constraint screw, respectively.

All screws on the closed-loop mechanism must be linearly related, so that

$$\sum_{j=1}^{g} \omega_j \$_j = 0, \tag{7}$$

where $\omega_j \left(j = 1, 2, \cdots, g\right)$ is the motion velocity of the jth joint of the closed-loop mechanism, and they are not all zero. In addition, $\$_j$ represents the motion screw of the jth joint.

By substituting Eqs. (3) and (4) into Eq. (7), one obtains

$$\sum_{i=1}^{l} \omega_{Ri} \boldsymbol{s}_{Ri} = 0, \tag{8}$$

$$\sum_{i=1}^{l} \omega_{Ri} \boldsymbol{s}_{0Ri} + \sum_{j=1}^{g-l} \omega_{Pj} \boldsymbol{s}_{Pj} = 0. \tag{9}$$

2.2 Planar Single-DOF Closed-Loop Mechanism

At present, typical engineering equipment is mainly a series structure, which is similar to a cantilever beam.

Under heavy loads, the end exhibits a larger disturbance. Introducing a closed-loop mechanism into the series structure is equivalent to adding a support to the cantilever beam. It can significantly improve the mechanical properties of the equipment and increase the stiffness of the mechanism [25]. Given the input and output constraints, designing a closed-loop mechanism to meet functional requirements has always been a serious problem in engineering.

In a single-DOF closed-loop planar mechanism, the number of overconstraints $\lambda \in \{3,4\}$. When λ=3, the constraint–screw system contains one independent force constraint and two independent couple constraints, which are described as

$$\begin{cases} \$_{r1} = (\boldsymbol{s}_{r1}; \boldsymbol{s}_{0r1}), \\ \$_{r2} = (0; \boldsymbol{s}_{r2}), \\ \$_{r3} = (0; \boldsymbol{s}_{r3}). \end{cases} \tag{10}$$

For revolute pairs, the condition in which the virtual work is zero can be described as

$$\begin{cases} \delta \boldsymbol{W}_1 = -a_1 \sin\alpha_1 = 0, \\ \delta \boldsymbol{W}_2 = \cos\alpha_2 = 0, \\ \delta \boldsymbol{W}_3 = \cos\alpha_3 = 0. \end{cases} \tag{11}$$

All revolute pairs must be perpendicular to the two independent coupled constraint screws and intersecting or parallel to the force constraint screws.

For prismatic pairs, the condition in which the virtual work is zero can be described as

$$\begin{cases} \delta \boldsymbol{W}_1 = \cos\alpha_1 = 0, \\ \delta \boldsymbol{W}_2 = \delta \boldsymbol{W}_3 \equiv 0. \end{cases} \tag{12}$$

The axes of all prismatic pairs are perpendicular to the force constraint screws and independent of the couple constraint screws.

$$g{=}d + 1 {=}7 - \lambda. \tag{13}$$

There are four kinematic pairs in the mechanism, which can be referred to as the RRRR, RRRP, RRPP, RPPP, and PPPP, where P represents the prismatic joint, and R represents the revolute joint. The RRRP institution is shown in Figure 2.

When $\lambda = 4$, $g = 7 - \lambda = 3$. The constraint–screw system may contain either one independent force constraint and three independent couple constraints (F1) or two independent force constraints and two independent couple constraints (F2).

Similarly, in F1, the revolute pairs cannot be perpendicular to the three independent couple constraint screws; therefore, there is no revolute pair in the mechanism. The axis of the prismatic pairs must be perpendicular to the force constraint — that is, the mechanism can only be PPP, as shown in Figure 3.

In F2, the revolute pairs must be perpendicular to the two independent coupled constraint screws and intersecting or parallel to the two force constraint screws. The closed-loop mechanism under this condition is a triangular stable structure, which does not satisfy the requirements.

2.3 Solution Model of Planar Single-DOF Closed-Loop Mechanism

The joint part of the single-DOF closed-loop planar mechanism is divided into the input, output, and intermediate joint parts. Input screw $\$_i{=}(\ 0\ 0\ a_1;\ b_1\ c_1\ 0\ )$ and output screw $\$_o{=}(\ 0\ 0\ a_2;\ b_2\ c_2\ 0\ )$, where a_1 and a_2 can be 1 or 0. The intermediate joint part can be divided into revolute screw $\$_{Ri}{=}(\ 0\ 0\ 1;\ y_{Ri}\ -x_{Ri}\ 0\ )$ and prismatic screw $\$_{Pi}{=}(\ 0\ 0\ 0;\ x_{Pi}\ y_{Pi}\ 0\ )$, where x_{Ri} and y_{Ri} represent the position of the revolute joint in the coordinate system, x_{Ri} and y_{Ri} represents the motion direction of the prismatic joint in the coordinate system, and $y_{Pi}^2 + x_{Pi}^2 = 1$.

$$\omega_i \$_i + \sum_{i=1}^{l} \omega_{Ri} \$_{Ri} + \sum_{i=1}^{m} \omega_{Pi} \$_{Pi} = \omega_o \$_o, \tag{14}$$

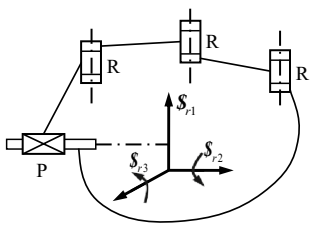

Figure 2 RRRP single-DOF closed-loop planar mechanism

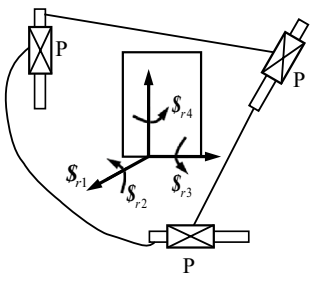

Figure 3 RRRP single-DOF closed-loop planar mechanism

where l and m are, respectively, the numbers of revolute pairs and prismatic pairs in the intermediate part, and $l+m \le 2$.

It can be deduced that

$$\sum_{i=1}^{l} \omega_{Ri} = a_2\omega_o - a_1\omega_i, \tag{15}$$

$$\sum_{i=1}^{l} y_{Ri}\omega_{Ri} + \sum_{i=1}^{m} x_{Pi}\omega_{Pi} = b_2\omega_o - b_1\omega_i, \tag{16}$$

$$-\sum_{i=1}^{l} x_{Ri}\omega_{Ri} + \sum_{i=1}^{m} y_{Pi}\omega_{Pi} = c_2\omega_o - c_1\omega_i. \tag{17}$$

According to Eq. (15), the number of revolute joints in the intermediate part for different input and output joints can be obtained ($\omega_{Ri} \neq 0$). When $a_i = 0$, the joint is a prismatic pair, and, when $a_i = 1$, the joint is a revolute pair.

The velocity relationship of the intermediate joint can be obtained by combining Eqs. (15, 16, 17).

$$\sum_{i=1}^{l}\left(\frac{a_2y_{Ri}-b_2}{a_1b_2-a_2b_1}+\frac{a_2x_{Ri}-c_2}{a_1c_2-a_2c_1}\right)\omega_{Ri} = \sum_{i=1}^{m}\left(\frac{a_2y_{Pi}}{a_1c_2-a_2c_1}-\frac{a_2x_{Pi}}{a_1b_2-a_2b_1}\right)\omega_{Pi}. \tag{18}$$

When the input and output joint types are known, Eq. (18) can be substituted into Eqs. (16) and (17), and the velocity relationship between the input and output joints for different intermediate joint types can be obtained.

When $l = 0$ and $m = 1$,

$$\omega_o = \frac{b_1y_P - c_1x_P}{b_2y_P - c_2x_P}\omega_i. \tag{19}$$

When $l = m = 1$,

$$\omega_o = \frac{-a_1\left(x_Px_R + y_Py_R\right) + b_1y_P - c_1x_P}{-a_2\left(x_Px_R + y_Py_R\right) + b_2y_P - c_2x_P}\omega_i. \tag{20}$$

When $l = 2$ and $m = 0$,

$$\omega_o = \frac{a_1\left(x_{R2}y_{R1} - x_{R1}y_{R2}\right) + b_1(x_{R1} - x_{R2}) + c_1\left(y_{R1} - y_{R2}\right)}{a_2\left(x_{R2}y_{R1} - x_{R1}y_{R2}\right) + b_2(x_{R1} - x_{R2}) + c_2\left(y_{R1} - y_{R2}\right)}\omega_i. \tag{21}$$

When $l = 0$ and $m = 2$,

$$\omega_o = \frac{\left(x_{P2}y_{P1} - x_{P1}y_{P2}\right)[a_1a_2(b_1b_2 + c_1c_2) - a_2a_2(b_1b_1 + c_1c_1)]}{\left(x_{P2}y_{P1} - x_{P1}y_{P2}\right)[a_1a_2(b_2b_2 + c_2c_2) - a_2a_2(b_1b_2 + c_1c_2)]}\omega_i. \tag{22}$$

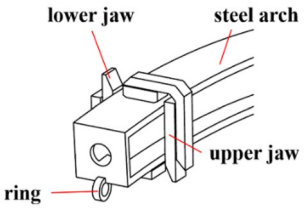

Figure 4 Schematic diagram of steel arch splicing

3 Design of Steel Arch Splicing Manipulator

A series of processes are carried out during the installation of TBM steel arches: transporting, grabbing, docking, and bracing. The designed steel arch splicing manipulator is divided into grasping and docking modules, where it is necessary to flexibly grasp, adjust, and connect two adjacent steel arches simultaneously. Moreover, in the process of steel arch transportation, the splicing manipulator does not interfere with the steel arch.

3.1 Design of the Grasping Module

As shown in Figure 4, a new form of steel arch was designed to facilitate the operation of the manipulator. A ring was welded to the bottom of the original steel arch end face. A manipulator was used to align the rings and connect them with bolts. This action was repeated until the steel arch was spliced into a split ring, and then, the bracing device was used on the TBM to brace the steel arch ring to the surrounding rock. Finally, the steel arch was sealed and formed into a ring to support it. According to the structure of the steel arch, it is envisaged to use two "L"-shaped jaws with a reverse arrangement to grasp the steel arch. Directly affected by the gravity of the steel arch, the lower jaw should be placed near the manipulator base when the gripping module is designed to provide better carrying capacity. To obtain a superior grasping effect, the lower jaws approach the steel arch directly below it. In addition, force sensor devices are needed by the mechanism to monitor the grasping force in real time and ensure the grasping performance of the steel arch splicing manipulator.

During the grasping process, the relative spatial positions of the upper and lower jaws must be adjusted to avoid collisions with the steel arch. Owing to the synchronizing movement, both jaws approach or move away from the steel arch simultaneously. If the upper jaw is envisaged to be driven by the movement of the lower jaw, then, considering the reduction in input control, a single-DOF closed-loop grasping module design scheme can be developed. The linear motion of the lower jaw serves as the input, and the motion of the upper jaw as the output. In particular, the output motion form can be regarded as a rotation or movement.

A plane coordinate system is established for the single-DOF closed-loop structure of a steel arch splicing manipulator. The lower jaw is set to move along the x-axis. When the output joint that drives the upper jaw is a revolute joint, the center of the revolute joint is considered to be the origin. However, when the output joint is a prismatic joint, the origin is determined as the intersection between the movement directions of the input and output prismatic joints. As shown in Figure 5, $\$_i$ is the input motion screw, which represents the screw of the lower jaw, $\$_i = \begin{pmatrix} 0 & 0 & 0; & 1 & 0 & 0 \end{pmatrix}$, and $\$_o$ is the output motion screw, i.e., the screw of the upper jaw.

When the output joint is a revolute pair, it can be seen from Figure 5a that the output screw $\$_{o1}$ is

$$\$_{o1} = \begin{pmatrix} 0 & 0 & 1; & 0 & 0 & 0 \end{pmatrix}. \tag{23}$$

At this point, $a_1 = 0$, $a_2 = 1$. According to Table 1, the number of revolute joints in the middle part is one or two. Combined with Eqs. (20) and (21), an eligible single-DOF closed-loop structure is obtained, as shown in Table 2.

When the output joint is a prismatic joint, the output screw $\$_{o2}$ can be obtained from Figure 5b as

$$\$_{o2} = \begin{pmatrix} 0 & 0 & 0; & 0 & 1 & 0 \end{pmatrix}. \tag{24}$$

At this point, $a_1 = a_2 = 0$. According to Table 1, the number of revolute joints in the middle part is zero or two. Combined with Eqs. (19)–(22), an eligible single-DOF closed-loop structure is obtained, as shown in Table 3.

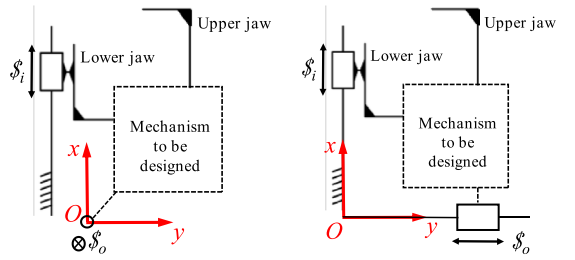

a Revolute output joint **b** Prismatic output joint

Figure 5 Schematic diagram of grasping module

Table 1 Number of revolute joints under different input and output joints

Input and output joint types	Condition	Number of rotating pairs
$a_1 = a_2 = 0$	$\sum_{i=1}^{l} \omega_{Ri} = 0$	$l \in \{0, 2\}$
$a_1 = 0, a_2 = 1$ or $a_1 = 1, a_2 = 0$	$\sum_{i=1}^{l} \omega_{Ri} \neq 0$	$l \in \{1, 2\}$
$a_1 = a_2 = 1$	$\sum_{i=1}^{l} \omega_{Ri} = \omega_o - \omega_i$	$l \in \{0, 1, 2\}$

The wear of the jaws and the size deviation of the steel arch can easily lead to insufficient grasping accuracy, resulting in the failure of the grasping force to meet the grasping requirements of the steel arch. With the addition of a prismatic DOF to the upper jaw, a force sensor is installed to guarantee the grasping effect. The four types of grasping module structure are illustrated in Figure 6.

3.2 Design of the Docking Module

Following the grasping action, a splicing manipulator is required to adjust and dock the steel arch. By driving the grasping module to complete the corresponding spatial rotation and lateral movement of the docking module, the grasping posture is adjusted, and the steel arch is docked. According to the action requirements of the docking module, the freedom space can be obtained by applying a graphical-type synthesis method. In addition, based on the functional equivalence of the space line diagram, the same-dimensional subspace of the docking module is derived, and the corresponding kinematic pair is also obtained, as shown in Figure 7.

3.3 Optional Configuration of Steel Arch Splicing Manipulator

By combining the grasping module and docking module, 12 basic structural forms of steel arch splicing manipulators that can meet the requirements of a single steel arch splicing motion were obtained, as shown in Figure 8.

All 12 steel arch splicing manipulators could realize the grasping and docking actions of the steel arch through distinct working methods, and the design requirements of the steel arch splicing manipulator could simultaneously be satisfied. However, owing to the differences in structure, each manipulator performed differently during manufacturing and construction. Therefore, the corresponding indices must be proposed and evaluated.

Table 2 Closed-loop structure of grasping module for revolute output joint

Number of intermediate kinematic pairs	Types of intermediate kinematic pair	Relationship to ω_i and ω_o	Grasping module closed-loop structure
2	2R	$\omega_O = \frac{x_{R1}-x_{R2}}{x_{R2}y_{R1}-x_{R1}y_{R2}}\omega_i$	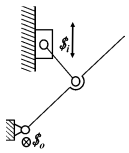
2	1R1P	$\omega_O = \frac{-y_P}{x_P x_R + y_P y_R}\omega_i$	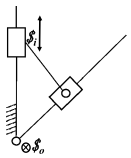

Table 3 Closed-loop structure of grasping module for prismatic output joint

Number of intermediate kinematic pairs	Types of intermediate kinematic pair	Relationship to ω_i and ω_o	Grasping module closed-loop structure
1	1P	$\omega_O = -\frac{y_P}{x_P}\omega_i$	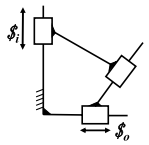
2	2R	$\omega_O = \frac{x_{R1}-x_{R2}}{y_{R1}-y_{R2}}\omega_i$	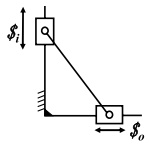
2	2P	$\omega_O = \frac{(x_{P2}y_{P1}-x_{P1}y_{P2})\times 0}{(x_{P2}y_{P1}-x_{P1}y_{P2})\times 0}\omega_i$	Ø: No solution to equation

4 Optimal Configuration of Steel Arch Splicing Manipulator

The steel arch splicing manipulator, as a heavy-duty manipulator used in tunnel engineering, must focus on the main performance indicators, such as strength, stiffness, working space, force/motion transfer, drive complexity, and structural complexity. However, the strength, stiffness, and performance indices of the manipulator are closely related to its rod length, section dimensions, and material parameters, which must be further considered in the subsequent dimension optimization design. In the initial configuration design process, the joint number, joint sequence and joint layout are mainly considered. Through the force/motion transmission index and complexity index, a manipulator with low topological complexity, low actuation-system complexity, and high transmission performance can be obtained to meet the engineering requirements [39].

4.1 Evaluation of Motion/Force Transmission Indices of Grasping Module

With the relatively complicated structure of the grasping module closed-loop mechanism, the motion/force transmission characteristics must be analyzed to ensure that the grasping requirements of the steel arch splicing manipulator can be satisfied.

4.1.1 Local Transmission Index

In the closed-loop mechanism of the grasping module, the kinematic pair screws, except the input screw $\$_i$ and output screw $\$_o$ are linearly independent, by which a screw system $\{\$_1, \cdots, \$_n\}$ could be formed. According to screw theory, the transmission force screw $\$_\mathrm{T}$ can be obtained, where $\$_\mathrm{T}$ is reciprocal to $\$_1$, ... ,$\$_n$ and independent of the linearity of the constraint–screw system of the closed-loop mechanism.

The input transmission coefficient ς and output transmission coefficient σ are defined, respectively, as [37

$$\begin{cases} \varsigma = \dfrac{|\$_i \circ \$_T|}{|\$_i \circ \$_T|_{\max}}, \\ \sigma = \dfrac{|\$_o \circ \$_T|}{|\$_o \circ \$_T|_{\max}}. \end{cases} \tag{25}$$

The local transmission index of the mechanism can be defined as

$$\chi = \min\{\varsigma, \sigma\}. \tag{26}$$

4.1.2 Global Transmission Index

The local transmission index can only judge the effectiveness of the motion and force transmission of the grasping module in a single posture. However, the grasping module operates in a continuous workspace. To judge the motion/force transmission in the entire working space, the global transmission index is defined as

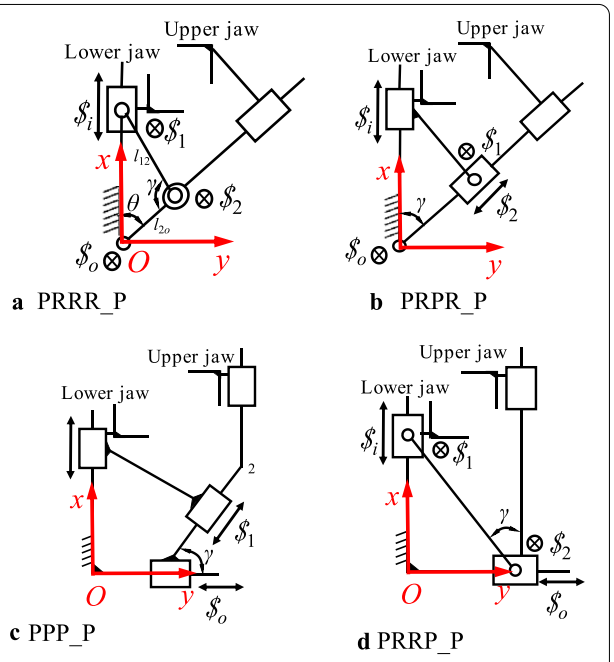

Figure 6 Optional structure of grasping module

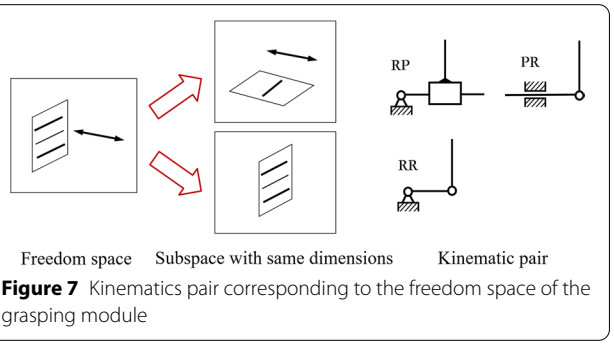

Figure 7 Kinematics pair corresponding to the freedom space of the grasping module

$$\boldsymbol{\Gamma} = \frac{\int_W \chi \, \mathrm{d}W}{\int_W \mathrm{d}W}, \tag{27}$$

where χ is the local transmission index, and W is the working space.

The motion/force transmission analysis was performed on the single-DOF closed-loop structures of the four types of grasping module. With the purpose of better motion/force transmission, the transmission angle γ adopts the most widely accepted range of 45° to 135°. As shown in Figure 6a, the grasping module is PRRR_P, $\theta \in [45°, 90°]$. To enable the transmission angle γ to satisfy the requirements and ensure transmission efficiency, it is necessary to set $l_{12} = \sqrt{2} l_{2o}$. The transmission performance of the closed-loop structures of the grasping module is shown in Table 4, where $(x_i \ y_i)$ is the position or movement direction of joint i in the coordinate system, l_{ij} is the distance between joints i and j, and the angles represented by θ and γ are shown in Figure 6.

The high-quality motion/force transmission mechanism is defined as a mechanism with a global transmission index $\boldsymbol{\Gamma}$, which is not less than 0.7. Table 4 shows that the grasping modules PRRR_P and PRPR_P are both high-quality motion/force transmission mechanisms.

4.2 Complexity Evaluation of Steel Arch Splicing Manipulator

In addition to the motion/force transmission performance, it is necessary to analyze the mechanical complexity of the steel arch splicing manipulator to obtain the best solution with low topology complexity, high performance, and low drive system complexity. The proposed structural complexity evaluation indices of the steel arch splicing manipulator are as follows.

(1) Joint number complexity K_N

$$K_N = 1 - \exp(-q_N N), \tag{28}$$

where N is the number of joints in the steel arch splicing manipulator, and q_N is the resolution parameter defined by

$$q_N = \begin{cases} -\ln(0.1)/N_{\max}, & \text{for } N_{\max} > 0; \\ 0, & \text{for } N_{\max} = 0. \end{cases} \tag{29}$$

(2) Joint-type complexity K_J

$$K_J = \frac{1}{n}\left(n_R K_{G|R} + n_P K_{G|P}\right), \tag{30}$$

where n_R and n_P are the numbers of revolute and prismatic joints, respectively, with $n = n_R + n_P$. Here, $K_{G|x}$ is the geometric complexity of pair x, as introduced elsewhere [39]: $K_{G|R} = 0.5234$, $K_{G|P} = 1$.

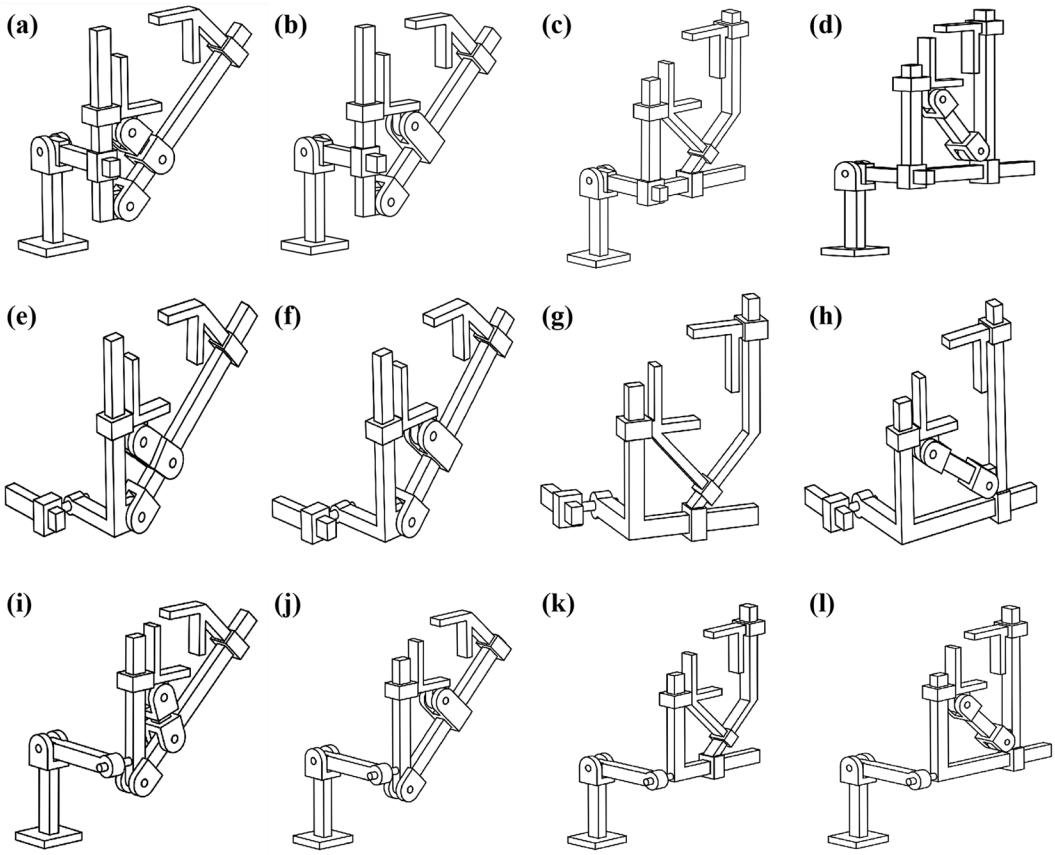

Figure 8 Single-side basic structures of steel arch splicing manipulators

Table 4 Motion/force transmission performance of the closed-loop structure of the grasping module

Type of grasping module	Expression of $\$_T$	Variable range	$\chi = \min\{\varsigma, \sigma\}$	Γ
PRRR_P	$\$_T = \left(x_2 - x_1 \;\; y_2 \;\; 0;\;\; 0 \;\; 0 \;\; x_1 y_2 \right)$	$\theta \in [45°, 90°]$	$\min\left\{ \frac{2\sqrt{3}}{3} \lvert\cos(\gamma + \theta)\rvert, \sin\gamma \right\}$	0.8803
PRPR_P	$\$_T = \left(-\sin\gamma \;\; \cos\gamma \;\; 0;\;\; 0 \;\; 0 \;\; \frac{y_1}{\sin\gamma} \right)$	$\gamma \in [45°, 90°]$	$\min\left\{ \sin\gamma, \frac{1}{\sqrt{2}\sin\gamma} \right\}$	0.7563
PPP_P	$\$_T = \left(-y_1 \;\; x_1 \;\; 0;\;\; 0 \;\; 0 \;\; 0 \right)$	$x_1 \in [0, l_{2o}\sin\gamma]$	$\min\left\{ 1, \frac{x_1}{l_{2o}\sin\gamma} \right\}$	0.5000
PRRP_P	$\$_T = \left(-x_1 \;\; y_2 \;\; 0;\;\; 0 \;\; 0 \;\; x_1 y_2 \right)$	$\gamma \in [45°, 90°]$	$\min\left\{ \sqrt{2}\cos\gamma, \sin\gamma \right\}$	0.4957

(3) Link diversity K_B

The link diversity K_B is defined to quantify the geometric constraints between neighboring joints. For a revolute joint, its axis of rotation is considered, whereas, for a prismatic joint, its direction is considered. Five possible joint constraint types between the neighboring joint axes/directions were reported previously [39].

Type B_1: Orthogonal intersection.

Type B_2: Nonorthogonal intersection.

Type B_3: Parallelism.

Type B_4: Orthogonal but not intersecting.

Type B_5: Skew.

Link diversity K_B of the steel arch splicing manipulator can be expressed as

$$K_B = \frac{B}{B_{\max}}, \quad B = -\sum_{i=1}^{c} b_i \log_2(b_i), \quad b_i = \frac{M_i}{\sum_{i=1}^{c} M_i}, \tag{31}$$

where B is the entropy of the joint constraint types, and $B_{\max} = 2.3219$ [40]. Here, c is the number of distinct

joint constraint types, and M_i is the instance number of each type of joint constraint.

(4) Actuator number complexity K_A

$$K_A = 1 - \exp(-q_A A), A = a - a_m, \tag{32}$$

where a is the number of actuators in the robot topology at hand, and a_m is the minimum number of actuators allowed.

$$q_A = \begin{cases} -\ln(0.1)/A_{\max}, & \text{for } A_{\max} > 0; \\ 0, & \text{for } A_{\max} = 0. \end{cases} \tag{33}$$

(5) Operation mode complexity K_{OM}

The operational complexity K_{OM} is specifically defined for a steel arch splicing manipulator. During the docking process of the steel arch, the designed steel arch splicing manipulators have two operation modes. In the first operation mode (OM1), the left and right docking modules drive a prismatic pair to drive the steel arch to dock along a straight line, as shown in the PR and RP structures in Figure 7. The second operation mode (OM2) simultaneously drives both revolute pairs at the same time, as shown in the RR structure in Figure 7. The motion trajectory is difficult to control with the application of the latter mode, and internal interference would also be likely. In this study, the problem was analyzed by introducing a new complexity index,K_{OM}.

$$K_{OM} = 0 \text{ for OM1}, \tag{34}$$

$$K_{OM} = 1 \text{ for OM2}. \tag{35}$$

(6) Total complexity K

The total complexity $K \in [0, 1]$ is defined as a convex combination of the different complexity indices. It is defined as

$$K = w_N K_N + w_J K_J + w_B K_B + w_P K_P + w_{OM} K_{OM}, \tag{36}$$

where w_N, w_J, w_L, w_B, w_P, and w_{OM} denote their corresponding weights, such that

$$w_N + w_J + w_B + w_P + w_{OM} = 1. \tag{37}$$

Assigning equal weights to all complexity indices implies

$$K = \frac{1}{5}(K_N + K_J + K_B + K_P + K_{OM}). \tag{38}$$

According to the evaluation results of the motion/force transmission indices of the grasping module, splicing manipulators a, b, e, f, i, and j had outstanding performance. The structural complexity analysis of the six steel arch splicing manipulators is shown in Table 5. Owing to the different operation modes of steel arch docking, the complexity of the latter two steel arch splicing manipulators is significantly higher than that of the first four. The complexity of manipulator j reached the highest value of 0.6911. In contrast, the complexity of the steel arch splicing manipulator b had the smallest value of 0.4228, primarily because of the smaller K_B and K_{OM} compared with other configurations, resulting in better performance.

After a comprehensive comparison between the motion/force transmission performance indices and complexity indices of the steel arch splicing manipulator, it was found that the work performance of steel arch splicing manipulator b was better than that of the others. Therefore, this is regarded as the optimal basic configuration.

4.3 Structure and Working Mode of Steel Arch Splicing Manipulator

A steel arch splicing manipulator is required to grasp two steel arches simultaneously; hence, manipulator b is arranged symmetrically. Because of the extremely narrow working space of steel arch splicing, it is necessary to transport and splice the steel arch. To avoid interference between the steel arch and manipulator during transportation, the designed splicing manipulator must be able to stay away from the steel arch transportation track. The complete structure of the steel arch splicing manipulator realized by means of joint rotation is shown in Figure 9.

Table 5 Complexity indices of the manipulators

	K_N	K_J	K_B	K_A	K_{OM}	K
a	0.9	0.7274	0.8277	0	0	0.4910
b	0.9	0.7957	0.4182	0	0	0.4228
e	0.9	0.7274	0.6555	0	0	0.4566
f	0.9	0.7957	0.5904	0	0	0.4572
i	0.9	0.6596	0.6555	0	1	0.6430
j	0.9	0.7274	0.8277	0	1	0.6911

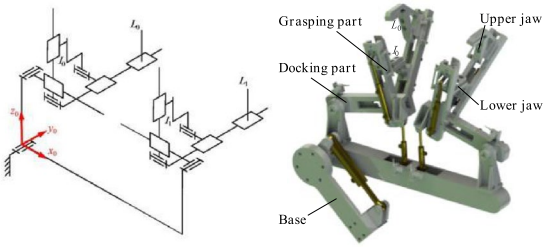

a Mechanism **b** Structure of steel arch splicing manipulator

Figure 9 Schematic diagram of steel arch splicing manipulator

Figure 10 shows the grasping and docking processes of the steel arch splicing manipulator. While transporting the steel arch, the manipulator rotated and was folded, as shown in Figure 10a. Driven by the oil cylinders, the lower jaws moved down, the upper jaws moved up, and the grasping modules opened to prepare for subsequent operations. Then, the manipulator reaches the designated position through the revolute joint, causing the steel arch to enter the grasping modules, as shown in Figure 10b. Subsequently, the upper jaws closed as the lower jaws moved upward to complete the grasping of the steel arch, as shown in Figure 10c. Simultaneously dragging the two grasped steel arches toward the middle, the docking operation of the steel arches was completed, as shown in Figure 10d.

5 Prototype Manufacturing and In-Plant Testing

5.1 Trial Production of Steel Arch Splicing Manipulator

Based on the research results, a prototype of the steel arch splicing manipulator was designed and manufactured [41]. The prototype was applied to a TBM in a TBM manufacturing plant. The position and pose of the jaws were controlled using a hydraulic cylinder. It can grasp, adjust, and dock the steel arch. To increase the grasping reliability of the manipulator, nylon plates were set at the upper and lower jaws to increase the friction on the surface and ensure that the steel arch did not slip during the docking process.

The distributions of the cylinders in the steel arch splicing manipulator are shown in Figure 11. According to the different functions, they can be divided into five types.

Cylinder No. 1 is the rotating cylinder of the steel arch splicing manipulator, which is used to control the steel arch splicing manipulator to avoid the transportation track of the steel arch.

Cylinder No. 2 is the posture adjustment cylinder, which is used to adjust the posture angle of the grasped steel arch.

Cylinder No. 3 is the docking cylinder, which is used to push the grasping modules to make docking operations for the steel arches possible on the two grasping modules.

Cylinder No. 4 is the lower jaw control cylinder, which is used to control the upward and downward movement of the lower jaw and simultaneously adjust the opening angle of the grasping module.

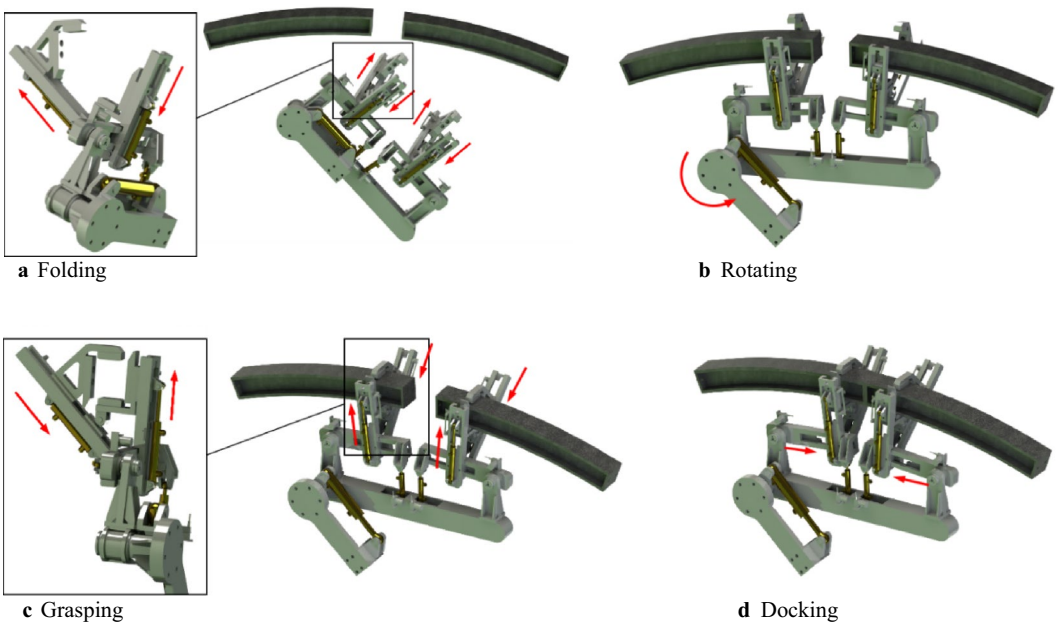

a Folding **b** Rotating

c Grasping **d** Docking

Figure 10 Working process of steel arch splicing manipulator

Figure 11 Steel arch splicing manipulator prototype

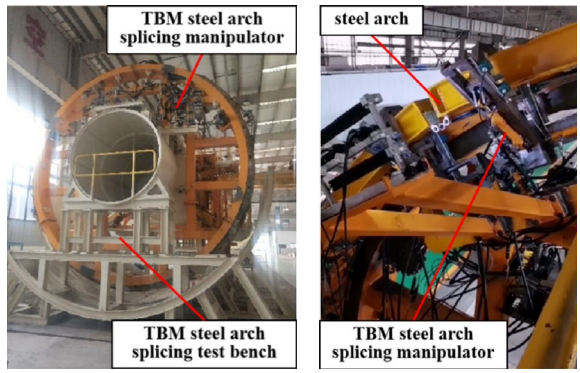

a Steel arch splicing test bench **b** Steel arch splicing test

Figure 12 TBM steel arch splicing test

Cylinder No. 5 is the upper jaw control cylinder, which is used to control the movement of the upper jaw and realize the grasping operation of the steel arch.

5.2 In-Plant Tests

The steel arch splicing manipulator prototype was used to perform steel arch grasping and docking experiments, as shown in Figure 12. When the manipulator is in contact with the steel arch, it is necessary to reduce the cylinder speed to ensure smooth operation. The motion control of each hydraulic cylinder during the experiment is listed in Table 6.

In the table, a positive number indicates cylinder stretch, while a negative number indicates cylinder contraction.

The splicing test of the two steel arches is divided into five stages: the No. 1 cylinders are stretched to realize the rotation of the splicing manipulator between 0 and 10 s. At 10–20 s, the No. 4 cylinders were contracted with the stretch of the No. 5 cylinders, while the jaws were expanded to prepare for the grasping of the steel arches. In the following period between 20 and 30 s, the stretch of the No. 2 cylinders enabled the jaws to be lifted and gradually approach the steel arches. At 30–50 s, the No. 4 cylinders were stretched, and the No. 5 cylinders contracted. At the same time, the tightened jaws would tightly hold the inside steel arches. Finally, at 50–70 s, the No. 3 cylinders were stretched, and the steel arches were pulled toward the middle to dock the steel arches.

Combined with Adams software and the input of the cylinder control parameters of each stage, the motion trajectory of the upper jaw L_0 and the lower jaw I_0 can be clearly obtained, as shown in Figure 13.

The motion trajectory of the upper jaw L_0 is similar to that of the lower jaw I_0; however, in stages 2 and 4, the upper jaw L_0 increases the motion along the z_0 axis, which is used to realize the separation and approach between the upper and lower jaws. During stage 3, the distance between I_0 and L_0 exceeds 400 mm, which is the farthest and is much larger than the steel arch width of 150 mm. Hence, technical requirements can be satisfied by avoiding collisions when the steel arch splicing manipulator approaches the steel arch. Moreover, at stage 5, where the steel arch splicing manipulator has grasped the steel arch, the distance between I_0 and L_0 in the horizontal and

Table 6 Control parameters of each cylinder at different stages

Stage	Time (s)	#1 ($mm \cdot s^{-1}$)	#2 ($mm \cdot s^{-1}$)	#3 ($mm \cdot s^{-1}$)	#4 ($mm \cdot s^{-1}$)	#5 ($mm \cdot s^{-1}$)
1	0–10	14	0	0	0	0
2	10–20	0	0	0	−12.5	12
3	20–30	0	13	0	0	0
4	30–50	0	0	0	6.25	−5
5	50–70	0	0	6.25	0	0

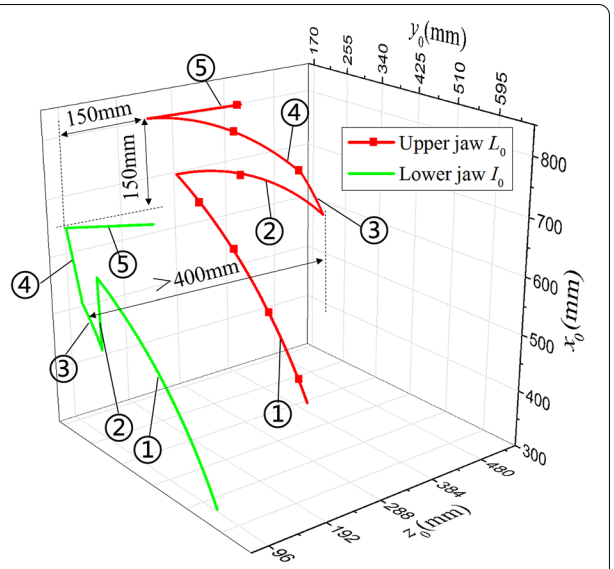

Figure 13 Motion trajectory of lower jaw l_0 and upper jaw L_0

vertical directions reaches 150 mm and meets the grasping conditions.

The experimental results show that the entire splicing process of the steel arches would occupy 70 s with a relatively high efficiency. During the grasping of the steel arches, there is no steel arch sliding or manipulator interference, which demonstrates the grasping effect. During the docking process, the alignment effect of the pinholes of the steel arch is excellent when the distance between the center axis of the hole is less than 5 mm, satisfying the accuracy requirements of the steel arch.

Regarding practical tunnel construction, the excessive weight of the steel arch increases the difficulty of manual handling and adjustment, in light of which even jacks and other devices would be needed for assistance. The manual connection of two adjacent steel arches would take approximately 5–10 min; in comparison, the splicing efficiency of the steel arch splicing manipulator is increased by four to eight times. Hence, the construction process could be significantly accelerated by the application of the splicing manipulator.

6 Conclusions

(1) To address the low efficiency of the manual installation of steel arches, a steel arch splicing manipulator with grasping and docking functions was developed. It is characterized by a simple structure, low manufacturing cost, and simple kinematic model, and it has good application prospects.

(2) Adding a single-DOF closed-loop mechanism increased the stiffness of the steel arch splicing manipulator grabbing module. A solution model for a single-DOF closed-loop mechanism was established. Under the condition that only the input constraints and output requirements are known, all grasping module configurations that meet the conditions were derived.

(3) Evaluation indices (motion/force transmission index and structural complexity index) in the configuration design process of the steel arch splicing manipulator were proposed, and the optimal configuration was derived from 12 optional manipulators.

(4) A prototype steel arch splicing manipulator was manufactured. Through the prototype test, the gripping effect, docking accuracy, and splicing efficiency of the manipulator met the design requirements. Compared with manual splicing for a steel arch, the splicing efficiency of the steel arch splicing manipulator was increased by four to eight times.

Acknowledgements
Not applicable.

Authors' contributions
YX and YH were responsible for the entire study; YH wrote the manuscript; ZX and JY assisted with sampling and field analyses; BN and XX assisted with modeling, data analysis, and manuscript writing. All authors have read and approved the final manuscript.

Authors' Information
Yuanfu He, born in 1995, is currently a PhD candidate at *College of Mechanical and Electrical Engineering, Central South University, China*. He received his master degree from *Central South University, China*, in 2020. His research interests include mechanical design and robotics.
Yimin Xia, born in 1967, is currently a professor at *College of Mechanical and Electrical Engineering, Central South University, China*. He received his PhD degree from *Central South University, China,* in 2006. His research intersts include large-scale tunneling equipment design, special robot.
Zhen Xu, born in 1981, is currently a senior engineer at *China Railway Construction Heavy Industry Co. Ltd, China*. He received his PhD degree in *South University, China*, in 2013. His research intersts include complexity system modeling and intelligent control, the design and manufacture of tunnel boring machine.
Jie Yao, born in 1982, is currently a senior engineer at *China Railway Siyuan Survey and Design Group Co. Ltd., China*. He received his PhD degree in *Wuhan University, China*, in 2010. His research interests include tunnel design, construction, and equipment applications.
Bo Ning, born in 1993, is currently a PhD candidate at *College of Mechanical and Electrical Engineering, Central South University, China*. His research intersts include dynamics, and rock breaking mechanism of disc cutters.
Xuemeng Xiao, born in 1996, is currently a PhD candidate at *College of Mechanical and Electrical Engineering, Central South University, China*. Her research intersts include design theory of fluid machinery for slurry shield.

Funding
Supported by Special funding support for the construction of innovative provinces in Hunan Province (Grant No. 2019GK1010), National Key R&D Program of China (Grant No. 2017YFB1302600).

Competing Interests
The authors declare no competing financial interests.

Author Details
[1]College of Mechanical and Electrical Engineering, Central South University, Changsha 410083, China. [2]State Key Laboratory of High Performance Complex Manufacturing, Central South University, Changsha 410083, China. [3]China Railway Construction Heavy Industry Co. Ltd., Changsha 410100, China. [4]China Railway Siyuan Survey and Design Group Co. Ltd., Wuhan 430063, China. [5]National-Local Joint Engineering Research Center of Underwater Tunnelling Technology, Wuhan 430063, China.

Received: 22 January 2021 Revised: 11 November 2021 Accepted: 18 February 2022
Published online: 05 April 2022

References

[1] J Z Huo, Z H Xu, Z C Meng, et al. Coupled modeling and dynamic characteristics of TBM cutterhead system under uncertain factors. *Mechanical Systems and Signal Processing*, 2020, 140: 106664.
[2] H D Yu, Y Y Li, L Li. Evaluating some dynamic aspects of TBMs performance in uncertain complex geological structures. *Tunnelling and Underground Space Technology*, 2020, 96: 103216.
[3] H S Gong, H B Xie, H Y Yang. A numerical method for extrication characteristics of TBM cutter-head with the HVC. *Chinese Journal of Mechanical Engineering*, 2019, 32: 102.
[4] Y P Shi, Y M Xia, Q Tan, et al. Distribution of contact loads in crushed zone between tunnel boring machine disc cutter and rock. *Journal of Central South University*, 2019, 26(9): 2393–2403.
[5] J F Tao, J B Lei, C L Liu, et al. Nonlinear static and dynamic stiffness characteristics of support hydraulic system of TBM. *Chinese Journal of Mechanical Engineering*, 2019, 32: 101.
[6] Y M Xia, B Guo, G Q Cong, et al. Numerical simulation of rock fragmentation induced by a single TBM disc cutter close to a side free surface. *International Journal of Rock Mechanics and Mining Sciences*, 2017, 91: 40–48.
[7] Y Zhu, W Sun, J Z Huo, et al. A new system to evaluate comprehensive performance of hard-rock tunnel boring machine cutterheads. *Chinese Journal of Mechanical Engineering*, 2019, 32: 103.
[8] R Zhang, G H Chen, J F Zou, et al. Study on roof collapse of deep circular cavities in jointed rock masses using adaptive finite element limit analysis. *Computers and Geotechnics*, 2019, 111: 42–55.
[9] O Rahaman, J Kumar. Stability analysis of twin horse-shoe shaped tunnels in rock mass. *Tunnelling and Underground Space Technology*, 2020, 98: 103354.
[10] A Mitelmam, D Elmo. Analysis of tunnel-support interaction using an equivalent boundary beam. *Tunnelling and Underground Space Technology*, 2019, 84: 218–226.
[11] Q J Chen, J C Wang, W M Huang, et al. Analytical solution for a jointed shield tunnel lining reinforced by secondary linings. *International Journal of Mechanical Sciences*, 2020, 185:105813.
[12] G L Zhong, Y D Hou, W Q Dou. A soft pneumatic dexterous gripper with convertible grasping modes. *International Journal of Mechanical Sciences*, 2019, 153–154: 445–456.
[13] C K Huang. A general method for developing different types of 3-DOF and 6-DOF isotropic manipulators. *Journal of the Chinese Society of Mechanical Engineers*, 2019, 40(2): 99–108.
[14] E Ozgür, G Gogu, Y Mezouar. A study on dexterous grasps via parallel manipulation analogy. *Journal of Intelligent and Robotic Systems*, 2017, 87: 3–14.
[15] P Lambert, J L Herder. A 7-DOF redundantly actuated parallel haptic device combining 6-DOF manipulation and 1-DOF grasping. *Mechanism and Machine Theory*, 2019, 134: 349–364.
[16] C Q Gao, H L Huang, B Li, et al. Design of a truss-shaped deployable grasping mechanism using mobility bifurcation. *Mechanism and Machine Theory*, 2019, 139: 346–358.
[17] D Y Liang, W Z Zhang. PASA-GB hand: A novel parallel and self-adaptive robot hand with gear-belt mechanisms. *Journal of Intelligent and Robotic Systems*, 2018, 90: 3–17.
[18] M M Kaluarachchi, J H Ho, S Yahya. Design of a single motor, tendon driven redundant manipulator with reduced driving joint torques. *Mechanics Based Design of Structures and Machines*, 2018, 46(5): 591–614.
[19] V Babin, C Gosselin. Picking, grasping, or scooping small objects lying on flat surfaces: A design approach. *The International journal of robotics research*, 2018, 37(12): 1484–1499.
[20] Q Yang, G B Hao, S J Li, et al. Practical structural design approach of multi-configuration planar single-loop metamorphic mechanism with a single actuator. *Chinese Journal of Mechanical Engineering*, 2020, 33: 77.
[21] C H Liang, M Ceccarelli, Y Takeda. Operation analysis of a Chebyshev-Pantograph leg mechanism for a single DOF biped robot. *Frontiers of Mechanical Engineering*, 2012, 7(4): 357–370.
[22] N G Lokhande, V B Emche. Mechanical spider by using klann mechanism. *International Journal of Mechanical Engineering and Computer Applications*, 2013, 1(5): 13–16.
[23] E Ottaviano, S Grande, M Ceccarelli. A biped walking mechanism for a rickshaw robot. *Mechanics Based Design of Structures and Machines*, 2010, 38(2): 227–242.
[24] J X Wu, Y N Yao, Q Ruan, et al. Design and optimization of a dual quadruped vehicle based on whole close-chain mechanism. *Proceedings of the Institution of Mechanical Engineers, Part C: Journal of Mechanical Engineering Science*, 2016, 231(19): 3601–3613.
[25] J X Wu, Y A Yao. Design and analysis of a novel multi-legged horse-riding simulation vehicle for equine-assisted therapy. *Proceedings of the Institution of Mechanical Engineers, Part C: Journal of Mechanical Engineering Science*, 2017, 232(16): 2912–2925.
[26] J X Wu, Y A Yao. Design and analysis of a novel walking vehicle based on leg mechanism with variable topologies. *Mechanism and Machine Theory*, 2018, 128: 663–681.
[27] Y J Liu, P Ben-Tzvi. An articulated closed kinematic chain planar robotic leg for high-speed locomotion. *Journal of Mechanisms and Robotics*, 2020, 12(4): 041003.
[28] A Hassan, M Abomoharam. Design of a single DOF gripper based on four-bar and slider-crank mechanism for educational purposes. *Procedia CIRP*, 2014, 21: 379–384.
[29] A Hassan, M Abomoharam. Modeling and design optimization of a robot gripper mechanism. *Robotics and Computer-Integrated Manufacturing*, 2017, 46: 94–103.
[30] M Anwar, T Khawli, I Hussain, et al. Modeling and prototyping of a soft closed-chain modular gripper. *Industrial Robot*, 2019, 46(1): 135–145.
[31] H D Yu, J Zhang, H Wang. Dynamic performance of over-constrained planar mechanisms with multiple revolute clearance joints. *Proceedings of the Institution of Mechanical Engineers, Part C: Journal of Mechanical Engineering Science,* 2018, 232(19): 3524–3537.
[32] Y Q Li, Y Zhang, L J Zhang. A new method for type synthesis of 2R1T and 2T1R 3-DOF redundant actuated parallel mechanisms with closed loop units. *Chinese Journal of Mechanical Engineering*, 2020, 33: 78.
[33] C C Zhou, Y F Fang. Design and analysis for a three-rotational-DOF flight simulator of fighter-aircraft. *Chinese Journal of Mechanical Engineering*, 2018, 31: 55.
[34] S F Yang, T Sun, T Huang. Type synthesis of parallel mechanisms having 3T1R motion with variable rotational axis. *Mechanism and Machine Theory*, 2017, 109: 220–230.
[35] T Sun, S F Yang, T Huang, et al. A finite and instantaneous screw based approach for topology design and kinematic analysis of 5-axis parallel kinematic machines. *Chinese Journal of Mechanical Engineering*, 2018, 31: 44.
[36] F G Xie, X J Liu. Design and development of a high-speed and high-rotation robot with four identical arms and a single platform. *Journal of Mechanisms and Robotics*, 2015, 7(4): 041015.
[37] F G Xie, X J Liu, C Wang. Design of a novel 3-DoF parallel kinematic mechanism: type synthesis and kinematic optimization. *Robotica*, 2015, 33(3): 622–637.
[38] K T Zhang, J S Dai. Geometric constraints and motion branch variations for reconfiguration of single-loop linkages with mobility one. *Mechanism and Machine Theory*, 2016, 106: 16–29.
[39] A Nayak, S Caro, P Wenger. Comparison of 3-[PP]S parallel manipulators based on their singularity free orientation workspace, parasitic motions and complexity. *Mechanism and Machine Theory*, 2018, 129: 293–315.
[40] S Caro, W A Khan, D Pasini, et al. The rule-based conceptual design of the architecture of serial schnflies-motion generators. *Mechanism and Machine Theory*, 2010, 45(2): 251–260.
[41] Y F He, Y M Xia, B Long, et al. Grasping docking mechanism of TBM steel arch splicing robot. *Journal of Zhejiang University: Engineering Science*, 2020, 54(11): 2204–2213. (in Chinese)